Quaternions and hybrid nematic disclinations

Simon Čopar[1,2] and Slobodan Žumer[1,3]

[1] *Faculty of Mathematics and Physics, University of Ljubljana, Jadranska 19, 1000 Ljubljana, Slovenia*

[2] *Department of Physics and Astronomy, University of Pennsylvania, 209 South 33rd Street, Philadelphia, Pennsylvania 19104, USA*

[3] *J. Stefan Institute, Jamova 39, 1000 Ljubljana, Slovenia*

(Dated: November 12, 2012)

Abstract

Disclination lines in nematic liquid crystals can exist in different geometric conformations, characterised by their director profile. In certain confined, colloidal and even more prominently in chiral nematics, the director profile may vary along the disclination line. We construct a robust geometric decomposition of director profile variations in closed disclination loops based on a quaternion description and use it to apply topological classification to linked loops with arbitrary variation of the profile. The description bridges the gap between the known abstract classification scheme derived from homotopy theory and the observable local features of disclinations. We compare the resulting decomposition of disclination loop features to a similar decomposition of nematic textures on closed surfaces.

I. INTRODUCTION

The defects in condensed materials have a significant effect on their physical properties. While their existence may be caused by impurities and flawed preparation process, controlled manipulation of defects can enable tuning of the physical characteristics of the material. The ability of a medium to host defects is a side-effect of symmetry breaking on the microscopic scale. As such, the defects are intimately related to the topological properties of degenerate microscopic degrees of freedom. In materials without broken translational symmetry, such as uniaxial and biaxial nematics [1], ferromagnets [2] and superfluid helium [3, 4], the defects can be roughly classified by their dimension into point defects, line defects and walls [5]. Their classification with the aid of homotopy groups is a well-established and efficient way of describing their interactions and the conservation rules they obey [6]. However, the topological analysis does not account for the fine geometric details, which are under control of the free energy.

Specifically for nematic braids – networks of closed nematic disclination lines [7–9] – recent development has shown that additional geometric constraints allow for a finer classification of nematic braids and simplifies the understanding of their rewiring [10, 11]. The constraint of a fixed $-1/2$ disclination profile that holds for nematic braids is not universal and does apply necessarily to some constrained [12] or chiral systems [13–15]. But even without constraints, it should still be possible to convey the topological information through the geometric primitives. In this paper, we demonstrate a formalism that can describe the most general types of nematic disclinations in terms of the local director behavior and enumerate them using quaternions. We show that our interpretation naturally extends the existing formalism for $-1/2$ disclination loops and reveal a connection between closed disclination loops and two-dimensional nematic textures.

II. OVERVIEW

Before introducing any new results, we shall briefly overview the existing theoretical background regarding nematic defect loops.

A nematic liquid crystal consists of elongated molecules that are locally orientationally aligned [1]. In a continuum approximation, the order is described by the director $\mathbf{n}$, a unit

vector field, pointing in the direction of average molecular orientation. The head-to-tail symmetry of the molecules causes the sign of the director to be ambiguous.

Topologically, the director field is a map from the coordinate space $\mathbb{R}^3$ to the real projective plane $\mathbb{R}P^2$ – the ground state manifold (GSM). The fundamental group $\pi_1(\mathbb{R}P^2) = \mathbb{Z}_2$ distinguishes disclination lines, where the director makes a half-turn around the disclination, from nondefect states, but makes no distinction between different disclinations [6].

Our specific interest is focused on disclination lines that are closed into a loop. Disclination loops may be linked by other disclinations or carry a topological point charge, measured by the second homotopy group. Closed loops therefore also carry an additional topological index $\nu \in \mathbb{Z}_4$. An established result shows [16–18], that a set of n disclinations obeys a law in the form

$$\frac{1}{2}\left(\sum_{i=1}^{n}\nu_i - 2\sum_{i>j}^{n}\mathrm{Lk}_{ij}\right) = q \mod 2, \tag{1}$$

where q is the topological point charge of the set of disclination loops, Lk_{ij} are linking numbers between loops and the indices i and j run over all the loops. Odd indices ν correspond to disclinations that are threaded by other disclinations an odd number of times while even indices correspond to those that are threaded by and even number, which also applies to unthreaded loops. This theory describes all existing topological properties of disclination loops. However, the index ν is an abstract attribute assigned to each of the loops, so the application to the systems that are found in experiments, simulations and theoretical models requires a way to relate this index to observable attributes.

If instead of a three-dimensional space, the molecules of the nematic are restricted to move and orient in a two-dimensional plane, the system exhibits point defects, which can have any half-integer winding number, the lowest ones being $-1/2$ and $+1/2$ [6]. These two-dimensional point defects represent a restricted set of cross sections the disclination lines in three dimensions can have. The topological equivalence of all disclination lines in the three-dimensional case is caused by the ability of the director to rotate through the third dimension. If the director is forced by the free energy minimization or geometric constrants to be perpendicular to the disclination tangent, which is excellently obeyed in well-researched nematic colloids [9, 19, 20], closed $-1/2$ disclination loops can be described as ribbons that follow the rotation of the profile. Ribbons can be assigned an invariant called the self-linking number Sl [21, 22], which in the case of $-1/2$ disclinations quantifies how many times the

three-fold disclination profile rotates around the tangent when we traverse the loop [10]. In a braid of many disclination loops, each self-linking number is of the form $\mathrm{Sl} = m/3$, where the numerator m is odd if the loop is threaded by an odd number of other disclinations, and even if the loop is linked by nothing or by an even number of disclinations. The self-linking numbers of a set of n disclination loops with a $-1/2$ profile obey a rule

$$\frac{3}{2}\left(\sum_{i=1}^{n}\mathrm{Sl}_i + \sum_{i\neq j}^{n}\mathrm{Lk}_{ij}\right) + n = q \mod 2, \tag{2}$$

that bears resemblance to the Jänich's rule (1). The integers Lk_{ij} are the linking numbers between loops and Sl_i are self-linking numbers of individual loops. The comparison of equations (1) and (2) suggests a connection between the index ν and the self-linking number. In the following section, we confirm and extend this notion to all disclination loops.

III. THE PROFILE CIRCLES AND QUATERNIONS

All disclinations in a 3D nematic have in common that the director on a test loop around the disclination traces an irreducible path in the ground state manifold (GSM). As the GSM is a sphere with additional condition of the antipodal points identified, the loop is topologically equivalent to a half of a great circle, which can be symmetrically extended to the full circle (Fig. 1). As the vicinity of the disclinations is subject to elastic free-energy restrictions, this is a quantitatively reasonable approximation.

A closed disclination loop can be wrapped in a torus, $S^1 \otimes S^1$, generated by revolving a disclination-encircling loop parameterized by u, around the disclination loop parameterized by v. For each value of v, the parameter u traces a different great circle in the GSM (Fig. 1a). Each circle is fully specified by its normal and a reference director at a chosen parameter, $u = 0$ (Fig. 1b,c). The sense of circulation around the circle is important and prescribes the sign of its normal. For example, the $-1/2$ profile corresponds to the normal of the circle being anti-parallel to the disclination tangent in the real space, as the director rotates in the opposite sense compared to the circulation of the enclosing loop (hence the minus sign in $-1/2$). The circle is invariant to rotations for π around its normal because each point in the real space maps to two antipodal points in the GSM.

Let the parametrization of the director field on the torus be $\mathbf{n}(u, v)$. When v changes, the circle rotates, so the director at all values of parameter u transform with the same rotation,

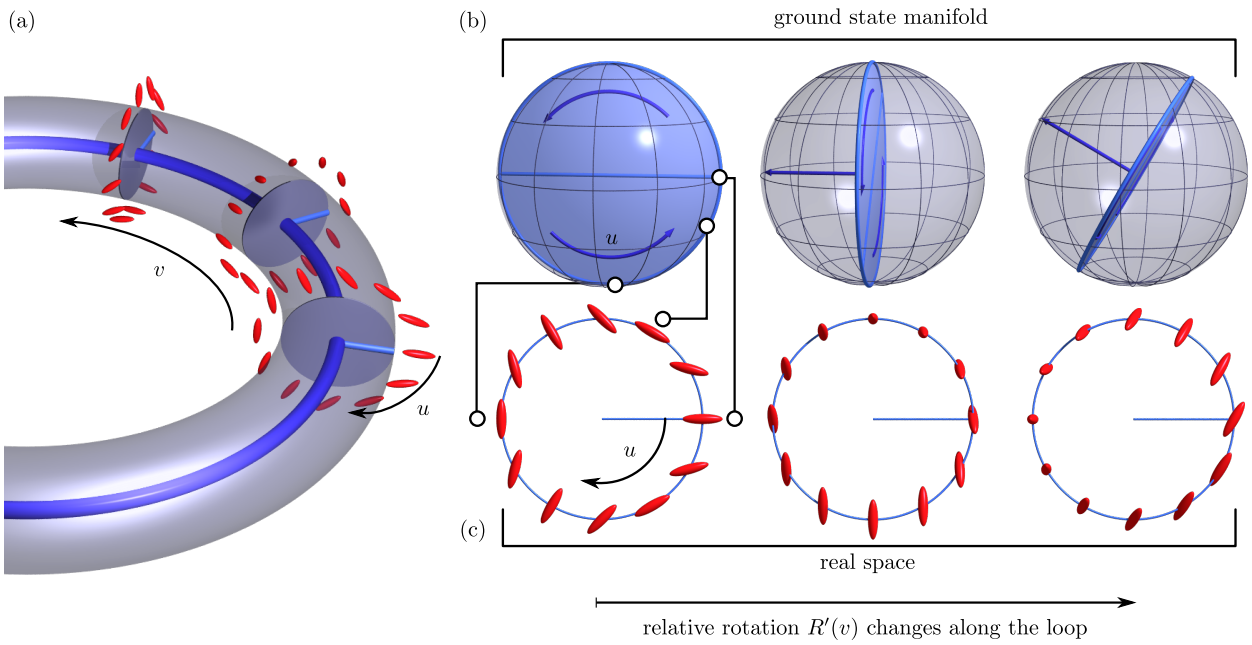

FIG. 1: (a) The director profile specified on a torus enveloping a general disclination loop. The small radius is parametrized by u and the large radius is parametrized by v, producing a seamless doubly periodic parametrization. (b) The director on any small cross section lies on a great circle in the GSM. The origin of the parameter $u = 0$ provides a reference in the plane of the circle and the sense of rotation in GSM with increasing u orients the circle's normal so that it defines a clockwise motion according to the right-hand rule. (c) Each circle in the GSM matches a cross section in real space with a fully specified parametrization u. (a-c) The orientation of the director cross section and its associated circle changes along the disclination with parameter v, which is described by a continuously changing rotation $\mathsf{R}'(v)$.

parameterized by v,

$$\mathbf{n}(u, v) = \mathsf{R}(v)\mathbf{n}(u, 0). \tag{3}$$

The $\mathbf{n}(u, 0)$ is simply a reference profile at a freely chosen point on the loop. This sets the initial rotation to unity, $\mathsf{R}(0) = 1$.

The rotations vary continuously with loop parameter v and thus describe a path in the space of all rotations in three-dimensions. We will use the quaternion representation of the SU(2) group. The unit quaternions $\mathbb{i}$, $\mathbb{j}$ and $\mathbb{k}$ obey the conventional structure relations $\mathbb{i}^2 = \mathbb{j}^2 = \mathbb{k}^2 = -1$, $\mathbb{ij} = -\mathbb{ji} = \mathbb{k}$, $\mathbb{jk} = -\mathbb{kj} = \mathbb{i}$ and $\mathbb{ki} = -\mathbb{ik} = \mathbb{j}$. A rotation around an

arbitrary axis $\mathbf{a}$ by an angle ϕ follows the usual spinor formula

$$\mathsf{R} = \cos\frac{\phi}{2} + (a_x\mathbb{i} + a_y\mathbb{j} + a_z\mathbb{k})\sin\frac{\phi}{2}. \tag{4}$$

Rotation by 2π around any axis yields $\mathsf{R} = -1$, which is the irreducible rotational motion that ends up in the same state where it started. Note that if we took the SO(3) representation, these irreducible paths would be considered equal to the identity transformation, and some of the topological information would be lost.

The continuity condition for a closed loop is satisfied if the director is continuous for *all* u, that is, if the circle we obtain after completing the loop at ($v = 2\pi$) matches the circle at the beginning of the loop ($v = 0$) up to a π rotation around the loop tangent, which we align with the z-axis. Because the SU(2) group covers the space of rotations twice, the set of possible cumulative rotations expands to

$$\mathsf{R}(v = 2\pi) \in \{1, \mathbb{k}, -1, -\mathbb{k}\} = \mathbb{k}^\nu. \tag{5}$$

The allowed rotations form a cyclic group $\mathbb{Z}_4$, enumerated by an integer ν, which can be shown to correspond to the index introduced by Jänich (1). As $\mathsf{R}(2\pi)$ is simply the total rotation of the director at any fixed u on a circuit around the disclination, it measures the fundamental group of the nematic encircled by the disclination. $\mathsf{R} = \pm\mathbb{k}$ are nontrivial rotations by π and mean the disclination is threaded by another disclination. $\mathsf{R} = 1$ and $\mathsf{R} = -1$ correspond to an unlinked loop with even and odd topological charge, respectively (this topic is discussed thoroughly in [18]).

Each rotation can be decomposed into the rotation $\mathsf{R}_0(v)$ of the local coordinate frame relative to the global coordinate frame, and the rotation $\mathsf{R}'(v)$ of the director relative to the local coordinate frame.

$$\mathbf{n}(u, v) = \mathsf{R}_0(v)\mathsf{R}'(v)\mathbf{n}(u, 0). \tag{6}$$

We set the local coordinate frame to keep its z-axis aligned to the disclination loop tangent and vary continuously along the loop (e.g. the Frenet-Serret frame). We also ensure our framing is topologically equivalent to a framing of a planar circular loop without torsion, so the local coordinate frame simply rotates by 2π when we traverse the loop: $\mathsf{R}_0(2\pi) = -1$. This extra rotational offset is present for all the loops, so we can factor it out. The multiplication of $\mathbb{k}^\nu$ by -1 simply shifts ν by 2 so an alternative parameter $\nu^* = \nu + 2$

mod 4 can be introduced, rewriting the Jänich's law (1) as

$$\frac{1}{2}\left(\sum_{i=1}^{n}\nu_i^* - 2\sum_{i>j}^{n}\mathrm{Lk}_{ij}\right) + n = q \mod 2. \tag{7}$$

We can see that the number of loops n plays a role in the conservation law because a trivial disclination loop with $\nu^* = 0$ holds a nonzero topological charge (one example is a Saturn ring defect). All the significant information is now encoded in $\mathsf{R}'(v)$, which is measured in a convenient disclination-aligned local coordinate frame.

IV. ALGEBRA OF PROFILE TRANSITIONS

Each geometric operation on the disclination profile can now be directly translated into the quaternion language. First, we reproduce the result for the $-1/2$ disclination profile. In the relative frame along the curve, the director lies in the xy plane and can only rotate around the z-axis, as it has to stay perpendicular to the disclination tangent. Rotation of the profile consists of both the passive rotation of the coordinate frame and the active rotation of the director. As the director lies in a plane, it can be specified by an angle α, so the profile rotation by ψ yields a $\phi = 3/2\psi$ rotation of the director, and subsequently the entire circle (Fig. 2a,b):

$$\alpha(u) = -\frac{1}{2}u; \quad \alpha'(u) = -\frac{1}{2}(u-\psi) + \psi = \alpha(u) + \underbrace{\frac{3}{2}\psi}_{\phi}. \tag{8}$$

In a loop with a self-linking number Sl, the profile rotates by a total angle of $\psi = 2\pi\,\mathrm{Sl}$, and the equation (4) gives

$$\mathsf{R}'(2\pi) = \cos\frac{3/2(2\pi\mathrm{Sl})}{2} + \mathbb{k}\sin\frac{3/2(2\pi\mathrm{Sl})}{2} = \mathbb{k}^{3\mathrm{Sl}}. \tag{9}$$

Comparison to $\mathbb{k}^{\nu^*}$ yields the index $\nu^* = 3\mathrm{Sl}$. The factor of 3 elegantly removes the fractional quantisation of the self-linking number that stems from the three-fold symmetry of the profile. This result immediately transforms the expression (7) to (2) and explains the correlation between the linking of disclinations and the self-linking number, discussed in Ref. [10].

A similar calculation yields $\phi = \psi/2$ and $\nu^* = \mathrm{Sl}$ for disclinations with a $+1/2$ profile.

There is more to disclinations than just rotations around the tangent. An obvious possibility is rotation around a perpendicular axis for $\phi = P\pi$, where $P = \pm 1$ is the parity

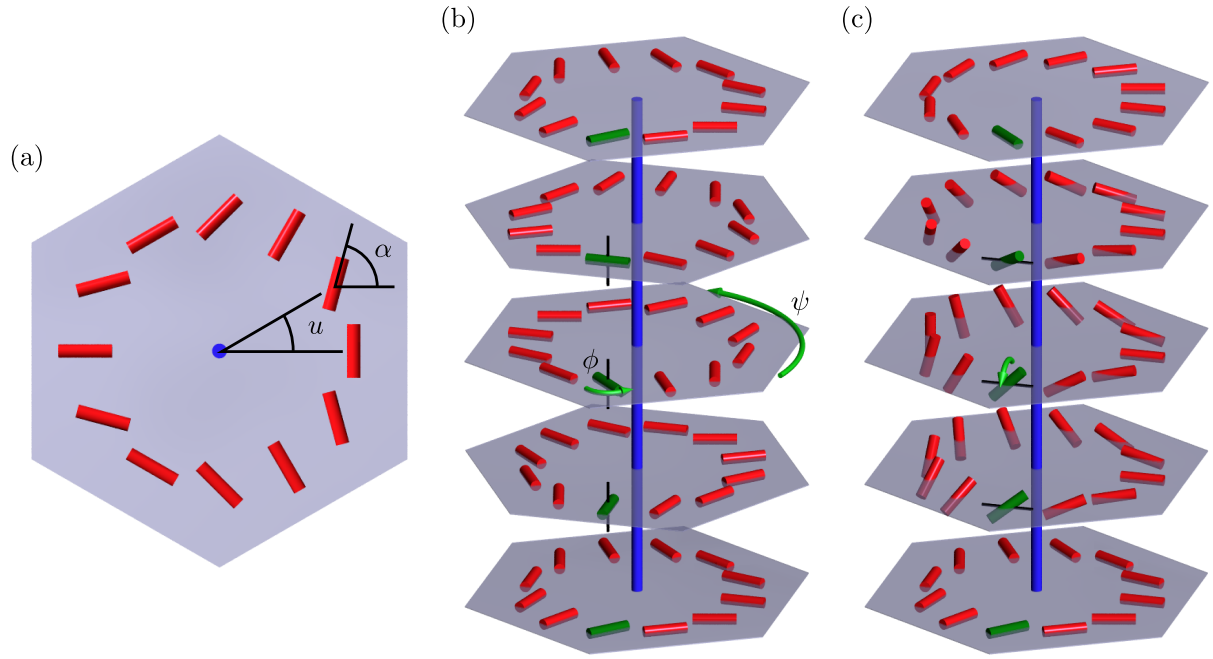

FIG. 2: (a) Notation used in equation (8). The $-1/2$ profile is two-dimensional, so the director can be represented by a single angle α that varies with parameter u. (b) Rotation of the director around the z axis induces a rigid rotation of the $-1/2$ disclination profile. Depicted is a rotation of the director for $\phi = \pi$, which yields a $1/3$ of a full turn for the profile ($\psi = 2\pi/3$). (c) The transition between $+1/2$ and $-1/2$ disclination profiles is realised by a rotation for π around a perpendicular axis (x axis, marked in black). There are two senses of rotation – the one depicted has the parity $P = +1$.

that distinguishes left-handed and right-handed rotation for π. The result of such a rotation is the transition between $+1/2$ and $-1/2$ defect profiles (Fig. 2c). The axis of rotation in equation (4) can point at any angle θ in the xy plane, $\mathbf{a} = (\cos\theta, \sin\theta, 0)$, which leads to

$$\mathsf{R}'_{\perp} = P(\mathbb{i}\cos\theta + \mathbb{j}\sin\theta) = P\mathbb{i}\exp(-\mathbb{k}\theta). \tag{10}$$

The rotations can be composed sequentially in the order they are encountered with increasing parameter v. A real disclination loop can have a profile that rotates around a gradually varying axis that is neither parallel nor perpendicular to the disclination tangent. However, the principal reasoning in our derivation is topological, so the exact geometric realisation of the rotations is not important. For example, the location of a transition between profiles can be pinpointed to the place where the circle's normal is exactly perpendicular

to the disclination's tangent. Whether the transition between $-1/2$ and $+1/2$ disclination profiles happens along a very short segment of the disclination, or takes the entire disclination length to complete, has no effect on the calculated index, as the director field in the second scenario can be smoothly combed to the first one without changing the topology. Consequently, rotations around the z axis (R'_z) and rotations for π around a perpendicular axis ($\mathsf{R}'_\perp$) are enough to describe all director profile variations:

$$\mathsf{R}'_z = \cos\frac{\phi}{2} + \mathbb{k}\sin\frac{\phi}{2} = \exp(\mathbb{k}\tfrac{\phi}{2}), \tag{11}$$

$$\mathsf{R}'_\perp = P(\mathbb{i}\cos\theta + \mathbb{j}\sin\theta) = P\mathbb{i}\exp(-\mathbb{k}\theta). \tag{12}$$

For the rotations R'_z, the angle ϕ is the local rotation angle of the director, which relates to the *physical* rotation angle ψ of the profile: $\phi = (3/2)\psi$ for a $-1/2$ profile and $\phi = (1/2)\psi$ for a $+1/2$ profile.

Because of the presence of the unit quaternion $\mathbb{i}$ in the perpendicular rotation, it does not commute with z-axis rotations.

$$\mathsf{R}'_z[\phi]\mathsf{R}'_\perp[\theta] = \mathsf{R}'_\perp[\theta]\mathsf{R}'_z[-\phi] \tag{13}$$

The rotation of $+1/2$ has the opposite effect than the rotation of $-1/2$ profile. The product of all local rotations must satisfy the continuity condition (5). As a perpendicular rotation introduces a factor $\mathbb{i}$, they must always appear in pairs – if the disclination turns from $-1/2$ to $+1/2$ it must turn back into $-1/2$. The offset in the axis orientations adds an extra amount of torsion,

$$\mathsf{R}'_\perp[P_1,\theta_1]\mathsf{R}'_\perp[P_2,\theta_2] = -P_1P_2\exp(\mathbb{k}(\theta_1-\theta_2)). \tag{14}$$

If two sequential rotations about the same perpendicular axis are performed with the same parity (twice by π or twice by $-\pi$), they yield

$$(\mathsf{R}'_\perp)^2 = -1, \tag{15}$$

which effectively changes the index ν^* by 2 and switches the topological charge between even and odd. Opposite parities naturally cancel out.

As an example, consider a disclination loop with a reference profile of $-1/2$ at $v = 0$, that rotates by ψ_1 around its tangent, flips to a $+1/2$ profile around an axis at an angle θ_1

and with parity P_1, then rotates by ψ_2 and flips back to $-1/2$ around an axis at θ_2 with parity P_2. The total rotation of the profile along the entire loop becomes

$$\begin{aligned}\mathsf{R}' =&(-P_1P_2)\mathbb{i}\exp(-\mathbb{k}\theta_2)\exp(\mathbb{k}\tfrac{\psi_2}{4})\mathbb{i}\exp(-\mathbb{k}\theta_1)\exp(\mathbb{k}\tfrac{3\psi_1}{4})\\ =&-P_1P_2\exp\left[\mathbb{k}\left(\frac{3}{4}\psi_1-\frac{1}{4}\psi_2+\theta_2-\theta_1\right)\right].\end{aligned}\tag{16}$$

The exponent must be a multiple of $\pi/2$ to satisfy the continuity equation, which puts a restriction on the angles $\phi_{1,2}$ and $\theta_{1,2}$. This generalises the third-integer quantization of the self-linking number. When this condition is met, the above expression can be compared to $\mathbb{k}^{\nu^*}$ to extract the index ν^*.

Note that the self-linking rotations of $+1/2$ and $-1/2$ parts have opposite-signed contributions to the index ν^*. Taking a different part of the loop as a reference cyclically permutes the order of the transformations. For example, if a $+1/2$ part serves as a reference, the entire exponent changes sign. This does not affect the $\mathsf{R}' = \pm 1$ rotations ($\nu^* \in \{0, 2\}$), but exchanges the signs of $\mathsf{R}' = \pm\mathbb{k}$ for linked disclinations. The same effect is observed if the parametrization of any of the disclination loops is reversed, which also reverses the linking numbers in equation (7). This ambiguity stems from the requirement of the classification with homotopy groups to have a fixed reference – a base point [6]. The choice of reference is very important once more than one loop is present in the system.

Most of the disclination loops can be analysed directly by the described formalism. Wherever the normal of the circle traced by the director on the unit sphere is not perpendicular to the disclination tangent, it can be simply regarded as being a $-1/2$ or a $+1/2$ profile and the director can be unambiguously combed to the perpendicular plane. The decomposition thus takes advantage of easily recognisable physical features of the disclination profiles and can be counted by hand if provided with a properly visualised director field. In singular cases, such as a twist disclination line, which is exactly half-way between $+1/2$ and $-1/2$ profiles, appropriate quaternion expressions can be quickly retrieved using a procedure similar to the one described above.

V. NEMATIC SURFACE TEXTURES

To present above statements from a different perspective, we must first shortly review the theory behind nematic point defects. The topological charge of a set of defects contained

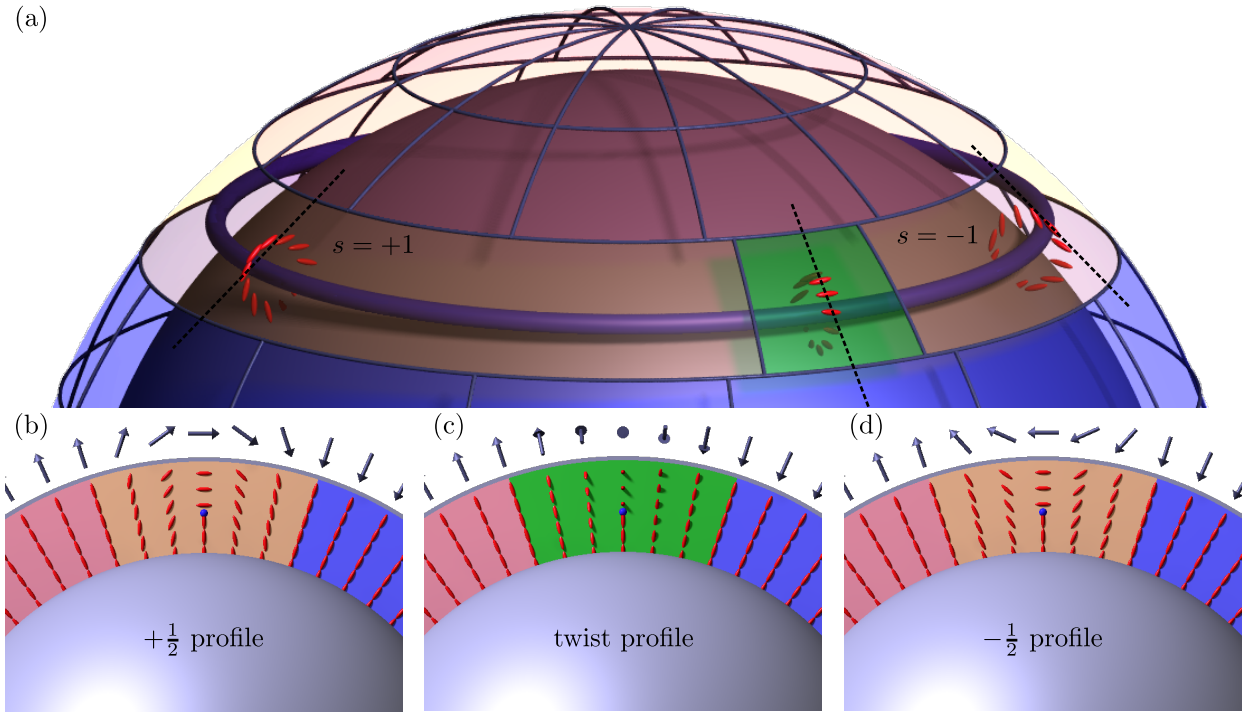

FIG. 3: The correspondence between subsurface disclination loops and geometric features of nematic textures on a sphere-like surface (a). The patches of perpendicular director (red for outgoing and blue for ingoing field) are segmented by boundaries (orange) with the director parallel to the surface. Boundary signature $s = \pm 1$ corresponds to $+1/2$ (b) or $-1/2$ (d) profiles of the subsurface disclination loops, while the grains – places where the director is parallel to the boundary – correspond to the twist profile, which is an intermediate state in transition between the other two elementary disclination profiles.

inside a surface is determined by the second homotopy group class of the nematic texture on said surface. A convenient way of calculating the topological charge is introduced in reference [23]. It states that a surface texture can be split into patches (2-dimensional objects) where the director is perpendicular to the enclosing surface, separated by boundaries (1-dimensional objects) where the director is parallel to the surface, but perpendicular to the boundary itself, and grains (isolated points on the boundaries) where the director is also parallel to the boundary of which it is part. The topological charge of the texture can then be calculated by counting the contributions of boundaries $t = \pm 1$ and grains $g = \frac{1}{2}$.

$$q = 1 + \sum_i t_i + \sum_j g_j \tag{17}$$

The first term is a half of the Euler characteristic of the enclosing surface and is related to the fact that a radial hedgehog has a topological charge of $q = 1$.

There is a striking similarity between the classification of disclination loops and the classification of nematic textures. Both theories observe the behaviour of the director in a local frame, aligned to the surface or the curve in question. This splits the global contribution of the shape's topology from the local geometric contributions. For disclination loops, the global part is the $\mathsf{R}_0 = -1$ factor that describes the nonzero topological charge of a simple Saturn ring defect, while for surface textures, it is the $+1$ contribution of the Euler characteristic that describes the nonzero topological charge of a radial hedgehog. Both approaches also assume the texture or the director profile can be smoothly transformed, so that all the changes happen in narrow transition zones.

The Figure 3 shows that every surface texture can be alternatively interpreted as a homeotropic core with added disclination loops below the surface of interest at the places where the boundaries are, and with disclination profile transitions where the grains are. The condition that the grains come in pairs and change the topological charge by 1 if they have the same parity, corresponds exactly to the same rule for the profile transitions. The topological charge of the texture can therefore also be calculated by adding the core $+1$ defect (the Euler characteristic) to the charges contributed by Jänich's indices for all the virtual subsurface disclination loops below the boundaries,

$$q = 1 + n + \sum_j g_j \mod 2, \tag{18}$$

for n boundaries and grains $g_j = \pm\frac{1}{2}$. One big difference between equations (17) and (18) is that the result is only given by modulo 2 in the latter. This is a natural consequence of dealing with line defects instead of point defects (see Ref. [18]). However, the narrow subset of disclinations that can act as subsurface representations of boundaries, are restricted by the surface of the homeotropic core, so there must be no linking and self-linking.

The correspondence between the textures and disclination loops is not necessarily only theoretical. If the surface on which we are observing the texture lies just above the disclinations, the geometric features on the surface texture will reflect the underlying disclination geometry. From this, another strong conclusion can be derived. The defect rank, a geometric measure for classifications of point charges, introduced in Ref. [23], is only valid if there are no grains on the surface. By the correspondence principle, we can state that if there are no

disclination transitions, no linking and no self-linking in the system, the defect rank can be used and the usual intuition of assigning proper integer charges to both disclination loops and point defects is valid. As soon as the system becomes entangled or there are different disclination profiles present in the system, there are possible discrepancies in the full integer conservation of the topological charge and only the even and odd conservation law holds.

VI. CONCLUSION

The topological properties of nematics are an interesting topic, crucial for interpretation and design of experiments. Although the basic, strictly topological formalism has been known for a long time, easy application of the theory to the real-world examples requires geometrization of the basic topological concepts. By considering local director behavior, we can account for restrictions enforced by the energy minimisation and thus make a fine-grained classification using not only the homotopy theory but also additional geometric information.

We have decomposed a general disclination loop into a sequence of local rotations that must add up continuously to a rotation that satisfies the director continuity in a closed disclination loop. Quaternions are an analytically efficient way of enumerating the local behavior of the director profile. The use of quaternions further reinforces the close relationship between the uniaxial and biaxial nematics, as the unified handling of the entire cross section removes the differences between both phases.

As an extension of the theory of $-1/2$ defects, the introduced formalism describes a wider range of disclination networks. Notable examples of systems that exhibit transitions between different director profiles are confined cholesteric phases [14, 15], optically induced defects [24] and transient defects that are created with quenching from the isotropic phase [25]. Studies of random blue phases [26] and entangled structures in random or structured pores [12] could also benefit from improved classification of disclination profile variations.

The formalism we presented also shows a stunning connection with the texture decomposition, suggesting that the approaches of geometrisation for different kinds of defects can be unified, leading toward a consistent set of tools for enumeration of defects.

VII. ACKNOWLEDGMENTS

This research was funded by Slovenian Research Agency under Contracts No. P1-0099 and No. J1-2335, NAMASTE Center of Excellence, and HIERARCHY FP7 network 215851-2. S. Č. was supported, in part, by NSF Grant DMR05-47230. Both authors also acknowledge partial support by NSF Grant PHY11-25915 under the 2012 KITP miniprogram "Knotted Fields".

---

[1] P. G. de Gennes and J. Prost, *The physics of liquid crystals* (Oxford University Press, 1993).

[2] P. R. Kotiuga, IEEE Trans. Magn. **25**, 3476 (1989).

[3] S. Blaha, Phys. Rev. Lett. **36**, 874 (1976).

[4] G. E. Volovik and V. P. Mineev, Sov. Phys. JETP **45**, 1186 (1977).

[5] M. Kleman, *Points, Lines and Walls: In Liquid Crystals, Magnetic Systems and Various Ordered Media* (1982).

[6] N. D. Mermin, Rev. Mod. Phys. **51**, 591 (1979).

[7] T. Araki and H. Tanaka, Phys. Rev. Lett. **97**, 127801 (2006).

[8] M. Ravnik and S. Žumer, Soft Matter **5**, 269 (2009).

[9] M. Ravnik, M. Škarabot, S. Žumer, U. Tkalec, I. Poberaj, D. Babič, N. Osterman, and I. Muševič, Phys. Rev. Lett. **99**, 247801 (2007).

[10] S. Čopar and S. Žumer, Phys. Rev. Lett. **106**, 177801 (2011).

[11] U. Tkalec, M. Ravnik, S. Čopar, S. Žumer, and I. Muševič, Science **333**, 62 (2011).

[12] T. Araki, M. Buscaglia, T. Bellini, and H. Tanaka, Nat. Mat. **10**, 303 (2011).

[13] J. Fukuda, Phys. Rev. E **81**, 040701 (2010).

[14] J. Fukuda and S. Žumer, Phys. Rev. Lett. **104**, 017801 (2010).

[15] J. Fukuda and S. Žumer, Phys. Rev. Lett. **106**, 097801 (2011).

[16] K. Jänich, Acta Appl. Math. **8**, 65 (1987).

[17] H. Nakanishi, K. Hayashi, and H. Mori, Commun. Math. Phys. **117**, 203 (1988).

[18] G. P. Alexander, B. G. Chen, E. A. Matsumoto, and R. D. Kamien, Rev. Mod. Phys. **84**, 497 (2012).

[19] I. Muševič, M. Škarabot, U. Tkalec, M. Ravnik, and S. Žumer, Science **313**, 954 (2006).

[20] S. Čopar, T. Porenta, and S. Žumer, Phys. Rev. E **84**, 051702 (2011).

[21] M. R. Dennis and J. H. Hannay, Proc. R. Soc. A **461**, 3245 (2005).

[22] W. F. Pohl, J. Mat. Mech. **17**, 975 (1968).

[23] S. Čopar and S. Žumer, Phys. Rev. E **85**, 031701 (2012).

[24] T. Porenta, M. Ravnik, and S. Žumer, Softmatter **8**, 1865 (2012).

[25] I. Chuang, B. Yurke, and A. N. Pargellis, Phys. Rev. E **47**, 3343 (1993).

[26] O. Henrich, K. Stratford, M. E. Cates, and D. Marenduzzo, Phys. Rev. Lett. **106**, 107801 (2011).